Inorganic Chemistry

Ba$_3$Fe$_{1.56}$Ir$_{1.44}$O$_9$: A Polar Semiconducting Triple Perovskite with Near Room Temperature Magnetic Ordering

Timothy Ferreira,[†] Darren Carone,[†] Amanda Huon,[§] Andreas Herklotz,[‡] Sebastian A. Stoian,[||] Steve M. Heald,[⊥][iD] Gregory Morrison,[†][iD] Mark D. Smith,[†] and Hans-Conrad zur Loye*,[†][iD]

[†]Department of Chemistry and Biochemistry, University of South Carolina, Columbia, South Carolina 29208, United States
[‡]Institute for Physics, Martin-Luther University Halle-Wittenberg, Halle 06120, Germany
[§]Department of Materials Science and Engineering, Drexel University, Philadelphia, Pennsylvania 19104, United States
[||]Department of Chemistry, University of Idaho, Moscow, Idaho 83844, United States
[⊥]X-ray Science Division, Advanced Photon Source, Argonne National Laboratory, Argonne Illinois 60439, United States

S *Supporting Information*

ABSTRACT: The crystal chemistry and magnetic properties for two triple perovskites, Ba$_3$Fe$_{1.56}$Ir$_{1.44}$O$_9$ and Ba$_3$NiIr$_2$O$_9$, grown as large, highly faceted single crystals from a molten strontium carbonate flux, are reported. Unlike the idealized $A_3MM'_2O_9$ hexagonal symmetry characteristic of most triple perovskites, including Ba$_3$NiIr$_2$O$_9$, Ba$_3$Fe$_{1.56}$Ir$_{1.44}$O$_9$ possesses significant site-disorder, resulting in a noncentrosymmetric polar structure with trigonal symmetry. The valence of iron and iridium in the heavily distorted Fe/Ir sites was determined to be Fe(III) and Ir(V) by X-ray absorption near edge spectroscopy (XANES). Density functional theory calculations were conducted to understand the effect of the trigonal distortion on the local Fe(III)O$_6$ electronic structure, and the spin state of iron was determined to be S = 5/2 by Mössbauer spectroscopy. Conductivity measurements indicate thermally activated semiconducting behavior in the trigonal perovskite. Magnetic properties were measured and near room temperature magnetic ordering (T$_N$ = 270 K) was observed for Ba$_3$Fe$_{1.56}$Ir$_{1.44}$O$_9$.

Fe1 full occupancy
0.14 Fe6: 0.86 Ir6
0.48 Fe5: 0.52 Ir5
0.71 Fe2: 0.29 Ir2
0.66 Fe4: 0.34 Ir4
0.11 Fe3: 0.89 Ir3
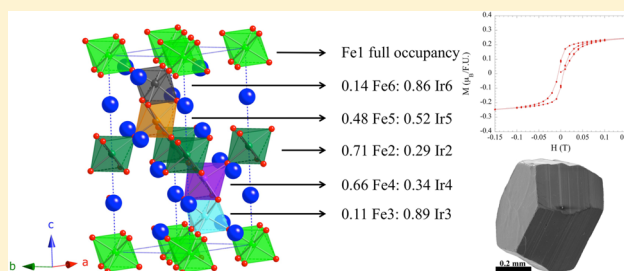
■ INTRODUCTION

The perovskite structure type is one of the most versatile structure types known to solid state chemistry, with reported cases of perovskites of diverse compositions crystallizing in all seven crystal systems.[1−11] This unique flexibility has given rise to a plethora of physical properties such as ferromagnetism,[12] ferroelectricity,[13] superconductivity,[14] metal-to-insulator transitions,[15] giant magnetoelastic effects,[16] and multiferroics[17] that serve as motivation for the continued study of complex perovskite oxides. The compositional versatility of the perovskite structure type stems from the variety of possible stacking sequences of [AO$_3$] layers, which serve as the building blocks with which the perovskite structures are generated. Cubic single (ABO$_3$) and double perovskites (A$_2$BB'O$_6$) are composed entirely of corner-sharing octahedra which are formed from close-packing [AO$_3$] layers in an ABC sequence, with the octahedral sites being occupied by the B site ion. By contrast, hexagonal single perovskites contain only face-sharing BO$_6$ octahedra due to close-packing of [AO$_3$] layers in an AB arrangement and the filling of the octahedral sites by the B site ion. More complex structures, such as triple (A$_3$BB'$_2$O$_9$) and quadruple (A$_4$BB'$_3$O$_{12}$) perovskites are generated by the simultaneous presence of both ABC and AB stacking sequences, resulting in combinations of both corner-sharing and face-sharing BO$_6$ octahedra. The ability of this structure

type to adopt an assortment of different stacking sequences and, in addition, accommodate a variety of metal cations, including those with unpaired electrons, in unique crystallographic positions with flexible bond angles, makes the perovskite family a convenient system with which to study structure−property relationships.

Triple perovskites, in particular, have been reported to adopt hexagonal, trigonal, orthorhombic, and monoclinic symmetries, in a large part due to their ability to host an extremely wide range of different-sized cations, including alkali, alkaline earth, and lanthanide metal cations on the A site, nearly any *d*-block element or lanthanide on the B and B' sites, and O$^{2−}$ and various chalcogenides and halides for the anionic site.[2−4,9,18−29] Such versatility, which has led to the observation of metallic conductivity,[18] giant magnetoelastic properties,[16] spin-liquid states,[30] and room temperature ferromagnetism[31] in perovskite materials, is inaccessible in most other solid state structures. The ease with which this structure type accommodates different elements allows the solid state chemist to judiciously select metal cations that are believed to be conducive to the creation of long-range magnetic order in crystallographic environments where magnetic interactions are possible. Considering the

idealized triple perovskite structure that has three crystallographically unique sites, the 12 coordinate A site, typically occupied by a larger (>1 Å) divalent nonmagnetic cation (primarily Ba^{2+} and sometimes Sr^{2+}), and the two B-sites, typically occupied the by a smaller di-, tri-, tetra-, or pentavalent cation. The latter sites consist of an isolated BO_6 octahedral environment and a face-sharing B'_2O_9 octahedral dimer site in which magnetic cations can be located. Most reported compositions contain a $3d$ metal cation on the BO_6 octahedral site that corner shares to a $4/5d$ metal cation occupying the B'_2O_9 dimers. For charge balancing reasons, the sum of the oxidation states of B and B' is limited to +12 when A = divalent. This often leads to divalent B sites and pentavalent B' sites, such as in $Ba_3CuRu_2O_9$[1] and $Ba_3NiIr_2O_9$.[19] Although less common, trivalent B sites and mixed-valent B' sites are known and include $Ba_3LnIr_2O_9$ and $Ba_3LnRuIrO_9$ (Ln = lanthanides, Y).[4,5]

Investigation of the magnetic properties of complex platinum group metal containing perovskites has been conducted for decades, both by our[3,5,6,8,10,22,23,32−39] and other groups.[1,2,4,7,9,12,16,18,19,21,24,25,27,28,40,41] Among these, iridates are of particular interest for their electrical and magnetic properties and, as a heavy $5d$ element, iridium experiences strong spin orbit coupling that competes with crystal field effects, causing observed physical properties to be highly sensitive to changes in the local chemical environment.[42] In a structure as easily tunable as a perovskite, there is significant interest in studying how changes in chemical environment manifest themselves in observed magnetic and electrical properties of iridates.[39,43−48] A study conducted by Jordan et al.[24] that investigated these effects in a family of hexagonal perovskites $BaIr_xFe_{1−x}O_{3−\delta}$ (x = 0.2, 0.3, 0.6) concluded that even a small difference in Ir content ($BaIr_{0.2}Fe_{0.8}O_{3−\delta}$ versus $BaIr_{0.3}Fe_{0.7}O_{3−\delta}$) resulted in significant variation of both structure and observed magnetic properties.

$BaIr_{0.2}Fe_{0.8}O_{3−\delta}$ is a typical 6H triple perovskite with $(hcc)_2$ stacking of AO_3 layers, while $BaIr_{0.3}Fe_{0.7}O_{3−\delta}$ is a less commonly observed 15R hexagonal perovskite with $(cchch)_3$ stacking of AO_3 layers, resulting in some B'_2O_9 dimers corner sharing with each other, instead of exclusively with BO_6 octahedra, as in the 6H triple perovskite. The significance of this study motivated the attempt to expand this family of iron and iridium containing hexagonal perovskites as single crystals. Herein we report on a novel triple perovskite, $Ba_3Fe_{1.56}Ir_{1.44}O_9$, synthesized as single crystals via a molten potassium carbonate flux. This composition, which was the result of the flux crystal growth and not a preselected composition, crystallizes in a unique noncentrosymmetric polar trigonal structure due to significant split-site occupancy. The fully ordered hexagonal triple perovskite $Ba_3NiIr_2O_9$ was also synthesized as single crystals from a molten carbonate flux to function as a reference material for iridium XANES and XPS studies. Herein we present the crystal growth, structure determination, oxidation state assignments, density functional theory calculations, Mössbauer measurements, conductivity, and magnetic properties of $Ba_3Fe_{1.56}Ir_{1.44}O_9$.

■ EXPERIMENTAL SECTION

Reagents. $BaCO_3$ (Alfa Aesar 99.95%), Fe_2O_3 (Alfa Aesar 99.5%), NiO_2 (Alfa Aesar, 99.99%), Ir powder (Engelhard, 99.9995%), and K_2CO_3 (BDH, ACS grade) were used as received.

Synthesis. Single crystals of $Ba_3Fe_{1.56}Ir_{1.44}O_9$ were grown from a high temperature potassium carbonate flux melt. $BaCO_3$ (3 mmol),

Fe_2O_3 (1 mmol), Ir (1 mmol), and K_2CO_3 (11g) were loaded into alumina crucibles with loose fitting alumina lids. The crucibles were heated to 1050 °C at 600 °C/h, held there for 10 h, slow cooled to 800 °C at 5 °C/h, and then allowed to cool to room temperature by turning off the furnace. The black hexagonal crystals were removed from the flux by dissolving the flux in water assisted by sonication. The crystals were isolated by vacuum filtration. Single crystals of $Ba_3NiIr_2O_9$ were grown using a procedure similar to the one used to grow $Ba_3Fe_{1.56}Ir_{1.44}O_9$ except for the substitution of Fe_2O_3 for NiO and a dwell temperature of 1150 °C, rather than 1050 °C.

Single Crystal X-ray Diffraction. The compound $Ba_3Fe_{1.56}Ir_{1.44}O_9$ crystallized as lustrous black hexagonal bipyramidal rods. X-ray intensity data from a cleaved fragment of approximate dimensions $0.04 \times 0.04 \times 0.03$ mm^3 were collected at 301(2) K using a Bruker D8 QUEST diffractometer equipped with a PHOTON 100 CMOS area detector and an Incoatec microfocus source (Mo Kα radiation, $\lambda = 0.71073$ Å). The data collection covered 99.9% of reciprocal space to $2\theta_{max} = 80.53°$, with an average reflection redundancy of 32.7 and $R_{int} = 0.039$ after absorption correction. The raw area detector data frames were reduced and corrected for absorption effects using the SAINT+ and SADABS programs. Final unit cell parameters were determined by least-squares refinement of 9875 reflections taken from the data set. Initial structural models for various solutions were obtained with either SHELXS or SHELXT or were taken from the literature.[49] Difference Fourier calculations and full-matrix least-squares refinement against F^2 were performed with SHELXL-2014[49] using the ShelXle interface.[50]

The compound crystallizes in the trigonal/hexagonal system. The pattern of systematic absences in the intensity data showed many strong violations among the classes 00l, $l \neq 2n$ and hhl, $l \neq 2n$, indicating no 6_3 and c-glide symmetry elements are present. Sixteen space groups are thereby possible. An initial solution was obtained in P3. Subsequently the ADDSYM program was used to suggest higher symmetry space groups.[51] Eventually the acentric group $P3m1$ (No. 156) was found to be the best description of the structure. The asymmetric unit in $P3m1$ consists of 18 atomic positions: six barium atoms, six iron or mixed iron/iridium sites, and six oxygen atoms. All barium and Fe/Ir positions have site symmetry $3m$: Fe1, Fe2/Ir2, Ba1, and Ba2 are located on site $1a$; Fe5/Ir5, Fe6/Ir6, Ba3, and Ba4 on site $1b$; Fe3/Ir3, Fe4/Ir4, Ba5, and Ba6 on site $1c$. Oxygen atoms O2, O5, and O6 are located on mirror planes (site $3d$) and O1, O3, and O4 are located on general positions (site $6e$). Iron/iridium site mixing was identified on five of the six transition metal sites by the behavior of the displacement parameters, which either refined to a zero volume if refined as pure Fe or became abnormally large if refined as pure Ir. Only site Fe1 refined to 100% iron. The other five sites were constrained to full site occupancy. The refined occupancies are Fe2/Ir2 = 0.714(4)/0.286(4); Fe3/Ir3 = 0.110(8)/0.890(8); Fe4/Ir4 = 0.66(1)/0.34(1); Fe5/Ir5 = 0.481(9)/0.519(9); Fe6/Ir6 = 0.142(7)/0.858(7). All atoms were refined with anisotropic displacement parameters. Isotropic restraints (SHELX ISOR instructions) were applied to oxygen atom O1 and O6 to prevent unacceptably flattened displacement ellipsoids. This is likely because of the pseudosymmetry of the structure, as discussed below. No deviation from full occupancy was observed for any of the barium atoms. Oxygen atom occupancies were not refined. The largest residual electron density peak and hole in the final difference map are +1.87 and −1.98 e$^-$/Å^3, located 0.04 Å from Fe3/Ir3 and 1.92 Å from O1, respectively. The crystal was a merohedral twin emulating the higher (hexagonal) Laue group. Data were refined with the twin matrix (−100/0−10/001), giving a major twin fraction 0.86(2). Each merohedrally related domain is further twinned by inversion, generating a total or four individual component domains in the crystal. The domain volumes refined to 0.53(2)/0.33(2) and 0.09(2)/0.05(2) for the two merohedral domains.

The structure is a lower-symmetry variant of the common 6H triple perovskite type with space group P6$_3$/mmc. In P6$_3$/mmc there are two symmetry-equivalent MO_6 octahedra (metal atoms at 000 and 001/2) and two symmetry-equivalent M_2O_9 face-shared bioctahedra per unit cell. Each M_2O_9 bioctahedron has one independent metal atom site, with the other being generated by the $-6m2$ site symmetry of the

group. The space group symmetry in $Ba_3Fe_{1.56(2)}Ir_{1.44(2)}O_9$ is lower because of partial ordering of Fe and Ir in the MO_6 and M_2O_9 octahedra, especially on the two MO_6 sites, and to a lesser extent on the M_2O_9 sites. Trial solution in $P6_3/mmc$ was clearly poor, with $R1 >$ 7% and large difference map extrema (*e.g.* + 8.5/−12.0 e$^-$/Å^3). In $P3m1$ (and $P-3m1$) the MO_6 octahedral sites Fe1 (at 0,0,z with z ∼ 0) and Fe2/Ir2 (0,0,z with z ∼ 1/2) are inequivalent because of different site composition (100% Fe and 71.4% Fe/28.6% Ir, respectively). This nonequivalence is the reason the aristotype ("$Ba_3FeIr_2O_9$") space group $P6_3/mmc$ is incompatible and why the strong 00*l* and *hhl* ($l \neq 2n$) systematic absence violations are observed (the 6_3 axis maps site 000 onto 001/2 *e.g.*). Other hexagonal space groups ($P6_3mc$, $P-6m2$, etc.) are incompatible because they also generate one unique MO_6 site or equivalent M_2O_9 sites per unit cell. Examination of the $P3m1$ structure suggests centrosymmetry. Adding an inversion center generates $P-3m1$. In $P-3m1$ the two MO_6 groups remain independent but equivalence is imposed on the two M_2O_9 units allowed in $P3m1$. The inversion symmetry of $P-3m1$ is therefore broken by the divergent occupancies primarily of the Fe4/Ir4 (0.66 Fe/0.34 Ir) and Fe5/Ir5 (0.52 Fe/0.48 Ir) bioctahedra. Solution and refinement in $P-3m1$ does produce good statistics ($R1 = 0.027/wR2 = 0.045$) but reflects the nonequivalent Fe/Ir sites in the large difference map features of +4.95 and −5.43 e$^-$/Å^3, located near Fe3/Ir3 and Fe4/Ir4, respectively. Because of better residuals, flatter residual electron density difference map, and the observation of nonequivalent Fe/Ir site occupancies, the acentric space group $P3m1$ was retained as a better description of the structure. The barium and oxygen substructures are compatible with various higher symmetry descriptions, which is likely the cause of the oxygen displacement parameter instability in the subgroup $P3m1$. The structure is therefore pseudosymmetric with small differences the Fe/Ir site mixing determining the correct symmetry.

X-ray intensity data from a lustrous black crystal of approximate dimensions 0.04 × 0.02 × 0.02 mm^3 were collected for $Ba_3NiIr_2O_9$ at 301(2) K using a Bruker D8 QUEST diffractometer equipped with a PHOTON 100 CMOS area detector and an Incoatec microfocus source (Mo Kα radiation, λ = 0.71073 Å). The data crystal was cleaved from a hexagonal bar. The data collection covered 100% of reciprocal space to $2\theta_{max} = 75.6°$, with an average reflection redundancy of 49.6 and $R_{int} = 0.0330$ after absorption correction. The raw area detector data frames were reduced, scaled, and corrected for absorption effects using the SAINT+ and SADABS programs. Final unit cell parameters were determined by least-squares refinement of 9972 reflections taken from the data set. An initial structural model was taken from the literature. Subsequent difference Fourier calculations and full-matrix least-squares refinement against F^2 were performed with SHELXL-2014[49] using the ShelXle interface.[50]

The compound crystallizes in the hexagonal system. The space group $P6_3/mmc$ (No. 194) was consistent with the pattern of systematic absences in the intensity data and was confirmed by structure solution. The compound adopts the hexagonal 6H triple perovskite structure type. The asymmetric unit consists of six atoms: two barium atoms (Ba1 on Wyckoff site 2*b* with site symmetry $-6m2$ and Ba2 on site 4*f* with site symmetry 3*m*), one nickel atom (site 2*a*, symmetry $-3m$), one iridium atom (site 4*f*, symmetry 3*m*), and two oxygen atoms (O1 on site 12*k* with symmetry *m* and O2 on site 6*h* with symmetry *mm*2). All atoms were refined with anisotropic displacement parameters. No deviation from full occupancy was observed for any of the metal atoms. The largest residual electron density peak and hole in the final difference map are +2.05 and −1.98 e$^-$/Å^3, both located <0.7 Å from Ir1. Crystallographic data are listed in Tables 1 and 2.

Energy Dispersive Spectroscopy (EDS). Single crystals of $Ba_3Fe_{1.56}Ir_{1.44}O_9$ and $Ba_3NiIr_2O_9$ were analyzed using a TESCAN Vega-3 SBU scanning electron microscope (SEM) with EDS capabilities. All crystals were mounted on carbon tape, and analysis was carried out using a 20 kV accelerating voltage and an accumulation time of 20 s. EDS verified the presence of Ba, Ir, and O and the respective transition metal element (Fe or Ni). The absence of

Table 1. Crystallographic Data for $Ba_3Fe_{1.56}Ir_{1.44}O_9$ and $Ba_3NiIr_2O_9$

Empirical formula	$Ba_3Fe_{1.56}Ir_{1.44}O_9$	$Ba_3NiIr_2O_9$
Formula Weight (g mol^{-1})	920.53	999.13
Space group	$P3m1$	$P6_3/mmc$
Unit cell dimensions		
a (Å)	5.7403(2)	5.7638(7)
c (Å)	14.1595(4)	14.3080(18)
V (Å^3)	404.06(3)	411.65(11)
Z	2	2
Density (calculated) (g cm^{-3})	7.566	8.061
Absorption coefficient (mm^{-1})	40.828	37
F(000)	783	844
Crystal size (mm)	0.04 × 0.04 × 0.03	0.04 × 0.02 × 0.02
Θ_{max} (deg)	40.265	37.817
Reflections collected	34268	24241
Independent reflections collected	2087 (R$_{int}$ = 0.0394)	471 (R$_{int}$ = 0.0330)
Goodness-of-fit on F^2	1.068	1.326
R indicies (all data)	R1 = 0.0247 wR2 = 0.0348	R1 = 0.0220 wR2 = 0.0456
Largest diff. peak.hole (e$^-$ Å^{-3})	1.875 and −1.983	2.048 and −1.978

Table 2. Interatomic Distance and Bond Valence Sum Values for M−Oxygen (M = Fe, Ni) and Iridium−Oxygen Bonds in $Ba_3Fe_{1.56}Ir_{1.44}O_9$ and $Ba_3NiIr_2O_9$

Empirical formula	Metal−Oxygen Bond	Bond Distance (Å)	Bond Valence Sum
$Ba_3Fe_{1.56}Ir_{1.44}O_9$	Fe1−O	1.996(5) × 3	2.95
		2.050(2) × 3	
	Ir3−O	1.981(11) × 3	4.95
		1.993(14) × 3	
	Ir6−O	1.940(13) × 3	5.01
		2.031(13) × 3	
$Ba_3NiIr_2O_9$	Ni−O	2.066(3) × 6	2.09
	Ir−O	1.923(3) × 3	5.14
		2.032(3) × 3	

extraneous elements, such as potassium, was confirmed within the detection limits of the instrument.

Electrical Resistivity. The electrical resistance of the single crystals was recorded as a function of the temperature by a two-probe method with the measurement along the thinnest side of the crystal (*a* axis). Silver paint electrodes were used as contact points. The temperature was controlled from 300 K down to 10 K in a Quantum Design PPMS while the resistance was measured with a Keithley 2450 Sourcemeter.

Density Functional Theory Calculations. Calculations were performed with ADF2014 software,[52] using a double-ζ DZP basis set with a small frozen core, and the PBESol[53] functional, using a spin-unrestricted formalism. The structure FeO$_6$ was capped with 6 hydrogens, constrained at the required symmetry. The calculations used 5 unpaired electrons and the total (−3) charge.

Mössbauer. The zero-field, room temperature ^{57}Fe Mössbauer spectrum was recorded using a spectrometer operated in a constant acceleration mode. The sample used in this study consisted of 50 mg of polycrystalline powder dispersed in eicosane contained in a custom-made polyethylene cup. The isomer shift is quoted against the centroid of a spectrum recorded at room temperature for a Fe metal foil.

Magnetic Susceptibility. Magnetic properties were measured on polycrystalline samples of $Ba_3Fe_{1.56}Ir_{1.44}O_9$ and $Ba_3NiIr_2O_9$ using a Quantum Design Magnetic Properties Measurement System (QD MPMS 3 SQUID Magnetometer). Magnetic susceptibility was

measured under zero-field cooled (zfc) and field cooled (fc) conditions from 2 to 400 K at an applied field of 0.1 and 1.0 T. Magnetization as a function of field was measured from 0 to 5 T at 2 and 45 K. Data were corrected for sample shape and radial offset effects as described previously.[54]

■ RESULTS AND DISCUSSION

Triple Perovskite Structure. Structurally, perovskites are composed of $[AO_3]$ layers that can stack in cubic close-packing arrangements to produce cubic single (ABO_3) or double ($A_2BB'O_6$) perovskites containing corner-shared octahedra or hexagonal closest-packing arrangements to produce hexagonal single perovskites (ABO_3) containing face-sharing octahedra. The mixing of both cubic (c) and hexagonal (h) close-packing layers of $[AO_3]$ leads to more complex structures, such as triple perovskites ($A_3BB'_2O_9$) that are composed of a $(hcc)_2$ stacking sequence, shown in Figure 1. In its ideal form, the triple
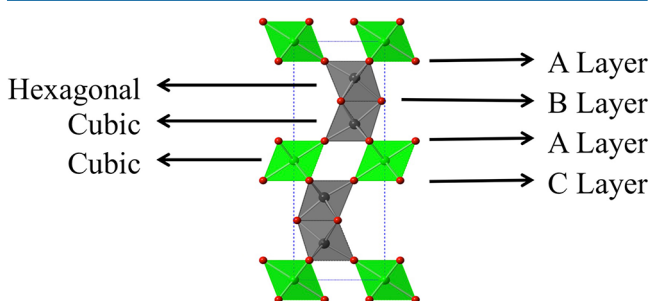
Figure 1. Polyhedral representation of an idealized hexagonal triple perovskite, with the BO_6 site shown in green as corner-sharing octahedra and the B'_2O_9 site shown in gray as face-sharing dimers. The stacking sequence of oxygen layers and resulting cubic or hexagonal closest-packing layers are indicated by black arrows.

perovskite contains a 12-coordinate A site, corner-sharing BO_6 octahedra formed from ABC stacking, shown in Figure 2A, and
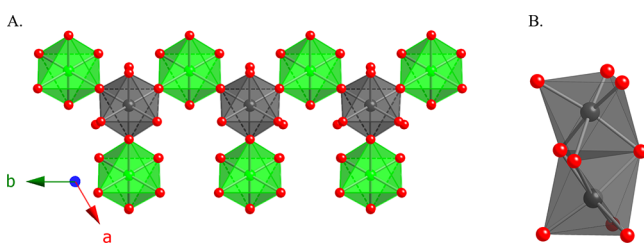
Figure 2. Polyhedral representation of the local coordination environments present in an idealized hexagonal triple perovskite. Corner-sharing BO_6 octahedra are shown in green (left), and face-sharing B'_2O_9 dimers are shown in gray (right).

B'_2O_9 face-sharing dimers resulting from AB stacking, shown in Figure 2B. In total, this high symmetry composition contains four crystallographically unique cationic sites: two A sites, one B site, and one B' site, most commonly crystallizing in the hexagonal space group $P6_3/mmc$, such as the herein reported $Ba_3NiIr_2O_9$, whose structure is shown in Figure 3, representing an ideal hexagonal triple perovskite.

As a compositionally versatile structure type, platinum group metal containing triple perovskites have been reported to crystallize in non-"idealized hexagonal" structures, such as the orthorhombic $Ba_3CuRu_2O_9$,[1] monoclinic $Ba_3LnIr_2O_9$,[4] or trigonal $Ba_3CaIr_2O_9$ structures.[9] The observation of three
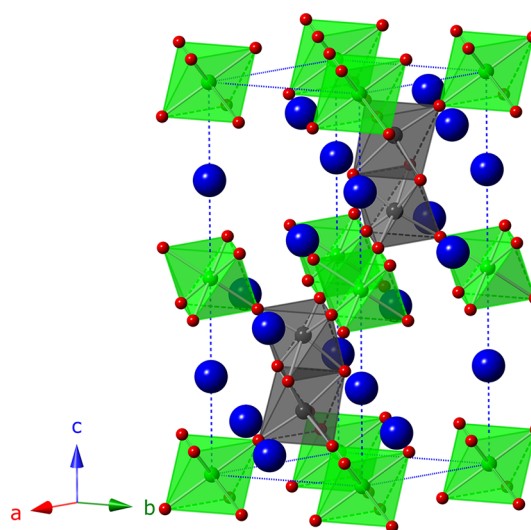
Figure 3. Polyhedral representation of the hexagonal $Ba_3NiIr_2O_9$, with barium shown as blue spheres, NiO_6 octahedra shown as green octahedra, and Ir_2O_9 dimers shown in gray.

different crystal systems for the same general structure type with similar A and B' sites indicates that the identity of the B site cation, in addition to the relationship between the relative sizes of the B and B' site, both strongly influence the resultant structure. For example, the composition $Ba_3NiRu_2O_9$[21] crystallizes in the commonly reported hexagonal $P6_3/mmc$ space group while $Ba_3CuRu_2O_9$ crystallizes in an orthorhombic space group due to Jahn–Teller distorted CuO_6. Similarly, $Ba_3LnIr_2O_9$ crystallizes as $P6_3/mmc$ for lanthanides smaller than Nd, but for Ln = La, Nd the structure is monoclinic. Similar to the monoclinic $Ba_3LaIr_2O_9$, the composition $Ba_3CaIr_2O_9$ is monoclinic under ambient conditions but is trigonal when synthesized under high pressure (5 GPa). Interestingly, trigonal perovskites are among the least reported for this structure type, and in this specific case resulted in the traditional B'_2O_9 units becoming individual $B'O_6$ units corner-shared to each other. It was reported that significant changes in electrical resistivity and magnetic susceptibility were reported as a result of this structural change. These examples are demonstrative of the chemical sensitivity of this structure and serve as the starting points from which solid state chemists can closely analyze and attempt to design reactions to bring about desired structures and properties.

The herein reported composition, $Ba_3Fe_{1.56}Ir_{1.44}O_9$, crystallizes in the noncentrosymmetric polar space group $P3m1$, and a scanning electron microscopy image of a crystal is shown in Figure 4. The reduction in symmetry and subsequent removal of inversion symmetry from the idealized $P6_3/mmc$ case is the direct result of significant site disorder, shown in Figure 5. Unlike the idealized hexagonal triple perovskite which contains two crystallographically unique B sites, one site for each B and B', this distorted trigonal variant contains six crystallographically unique sites in which five of them contain both Fe and Ir on the same site, with the sixth site fully occupied by iron. The conventional BO_6 corner-shared octahedron found in hexagonal perovskites has become two unique octahedral sites in this trigonal variant, one with full iron occupancy, and the other with a 0.71Fe2/0.29Ir2 split occupancy. Also, unlike ideal triple perovskites, the BO_6 polyhedra do not possess local O_h symmetry, but rather possess local C_{3v} symmetry, shown in
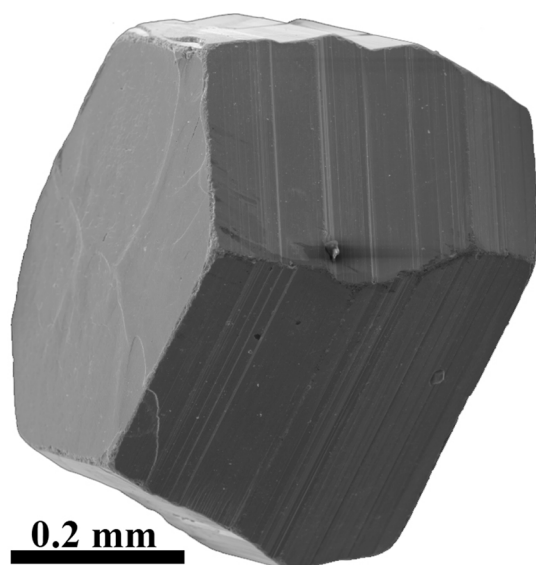
Figure 4. Scanning electron micrograph of $Ba_3Fe_{1.56}Ir_{1.44}O_9$.

Fe1 full occupancy

0.14 Fe6: 0.86 Ir6

0.48 Fe5: 0.52 Ir5

0.71 Fe2: 0.29 Ir2

0.66 Fe4: 0.34 Ir4

0.11 Fe3: 0.89 Ir3
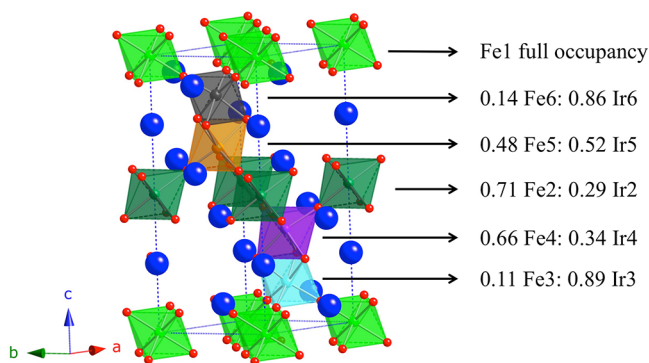
Figure 5. Polyhedral representation of the hexagonal $Ba_3Fe_{1.56}Ir_{1.44}O_9$, with barium shown as blue spheres, $Fe1O_6$ polyhedra shown in light green, the iridium-rich Ir6/Fe6 site shown as a gray polyhedra, the nearly equal mix of Ir5/Fe5 site shown as an orange polyhedra, the iron rich Fe2/Ir2 site shown as dark green polyhedra, the mixed Ir4/Fe4 site shown as a purple polyhedron, and the iridium rich Ir3/Fe3 site shown as a light blue polyhedron.

Figure 6, which is consistent with the Schönflies point group associated with $P3m1$. Although it is expected for there to be irregular BO_6 polyhedra due to site-disorder, $Fe1O_6$ is fully occupied and yet still exhibits two shorter equatorial bonds and one shorter axial bond, indicating a shift of the Fe cation toward one of the polyhedral faces, resulting in this local C_{3v} symmetry. The idealized B'_2O_9 units contain split occupancy and are split into four unique sites for this composition, two of which are iridium rich (0.86Ir6/0.14Fe6; 0.89Ir3/0.11Fe3) and two of which are more evenly split between iron and iridium (0.52Ir5/0.48Fe5; 0.34Ir4/0.66Fe4).

The observation of a noncentrosymmetric space group is uncommon, particularly in perovskites, but is of great interest for various practical applications, such as ferroelectricity. The physical properties of acentric compositions are symmetry-dependent and thus can be predicted based on the Hermann–Maugin or Schönflies symbols, best described by Glazer and Poeppelmeier.[55,56] The composition $Ba_3Fe_{1.56}Ir_{1.44}O_9$ crystallizes in the space group $P3m1$, which corresponds to the polar crystal class $3m1$ (C_{3v} in Schönflies notation). Less than half of all acentric crystal systems (21) are polar (10), showcasing the
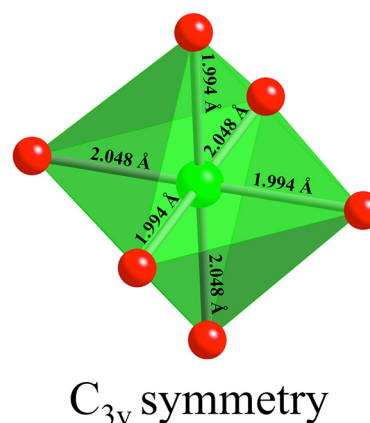
C_{3v} symmetry

Figure 6. Polyhedral depiction of $Fe1O_6$ in $Ba_3Fe_{1.56}Ir_{1.44}O_9$, indicating the local C_{3v} symmetry expected for the trigonal space group $P3m1$. Two equatorial bonds and one axial bond are shortened, indicating a shift of the Fe cation toward one face of the polyhedra.

rarity of this class of material. Polar materials are chiefly characterized as pyroelectric materials but are symmetry-allowed to exhibit piezoelectricity, second-harmonic generation, and ferroelectricity.[56] As a result, there was significant interest in measuring the electrical conductivity of the titled composition to see if ferroelectric measurements were suitable for study. This was further motivated by the possible existence of magnetic order due to the presence of two cations with unfilled d shells, as materials with simultaneous ferroelectric and ferromagnetic order are scarce and technologically useful.[57,58] Therefore, before either electrical or magnetic property measurements were undertaken, the electronic structure was clarified by assigning oxidation states in both titled compositions, particularly $Ba_3Fe_{1.56}Ir_{1.44}O_9$, as split-site occupancy introduced uncertainty in the oxidation state assignments.

Oxidation States. To determine the oxidation states of Ir and the respective first row transition metal cation in the triple perovskites, bond valence sum (BVS) analysis and X-ray absorption near edge spectroscopy (XANES) were performed. The ideal hexagonal triple perovskite $Ba_3NiIr_2O_9$ contains Ir in a similar chemical environment and thus was synthesized for comparative purposes. The results of the BVS analysis are shown in Table 2, indicating the presence of Ni(II) and Ir(V) for $Ba_3NiIr_2O_9$. Due to split-site occupancy, BVS was only utilized on select sites in $Ba_3Fe_{1.56}Ir_{1.44}O_9$, as the presence of multiple cations on one site makes BVS unreliable. Of the six unique sites, Fe1 was fully occupied by iron and thus BVS was most reliable, indicating Fe(III), with a value of 2.95. For charge balancing reasons, this suggests the presence of Ir(V), which was supported by BVS values of 4.95 and 5.01 for sites Ir3 and Ir6, respectively. It should be noted that neither site is fully occupied by iridium, but Ir3 consists of 89% iridium and Ir6 consists of 86% iridium, making BVS still fairly demonstrative of the oxidation state of iridium.

To further corroborate the BVS analysis, XANES measurements were taken of both compositions. The ideal hexagonal perovskite was synthesized as an appropriate model for the XANES spectrum of Ir(V) in a bioctahedron environment, typical of the triple perovskite structure type. As Fe(IV) and Ir(IV) or Fe(III) and Ir(V) were both plausible possibilities for the trigonal perovskite, the similarity of the XANES data for both compositions would support the presence of Fe(III) and

Ir(V) in the trigonal variant. The simple oxide Ir(IV)O$_2$ was included as a reference material in the XANES data to estimate the valence of Ir if the trigonal perovskite XANES data differed from the hexagonal one. The observation of a lower binding energy in the trigonal perovskite compared to the hexagonal perovskite, thus closer in binding energy to IrO$_2$, would be indicative of Ir(IV) or mixed Ir(V) and Ir(IV), whereas a higher binding energy would indicate a valence greater than Ir(V), which is uncommon, but reported cases exist.[59] The XANES data is shown in Figure 7, indicating identical binding energies
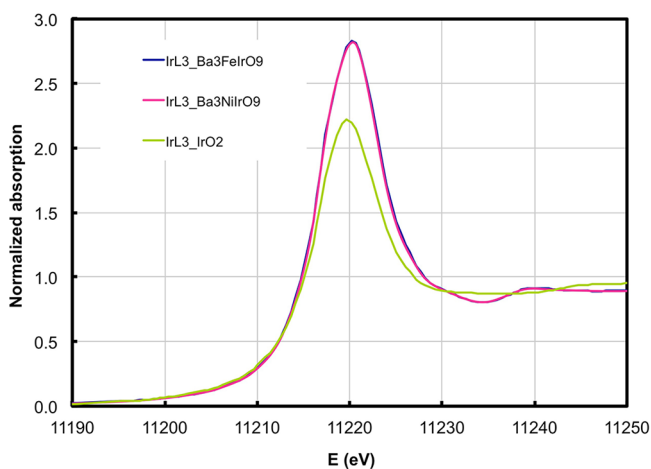
Figure 7. X-ray absorption near edge spectroscopy measurement of binding energies for the Ir L$_3$ edge plotted against normalized absorption for Ba$_3$Fe$_{1.56}$Ir$_{1.44}$O$_9$, Ba$_3$NiIr$_2$O$_9$, and IrO$_2$.

on the Ir L$_3$ edge for both compositions, confirming the assignment of Ir(V), thus supporting the presence of Fe(III) in the trigonal variant due to charge balancing and BVS analysis.

Electrical Conductivity. The temperature dependence of the electrical resistivity for Ba$_3$Fe$_{1.56}$Ir$_{1.44}$O$_9$ is shown in Figure 8. The decrease in electrical resistance as a function of temperature rules out metallic behavior, suggesting the titled material is either an insulator or a semiconductor. At 300 K, the material exhibited a resistance of 389 Ohms, which is low among oxide materials, supporting semiconducting behavior. Although this resistivity is low, similar trigonal triple perovskites such as Ba$_3$CaIr$_2$O$_9$, which crystallizes in the space group $P-3m1$, a centrosymmetric variant of the titled material, was reported to have a room temperature resistance on the same order of magnitude.[9]

The conduction mechanism was investigated by plotting the natural logarithm of resistance against T^{-n}, as the value of n can help identify both the type and dimensionality of the transport mechanism. A linear plot of Ln ρ vs T^{-1} is indicative of simple thermally activated conduction, corresponding to a case of n = 1. Linear plots of Ln ρ vs T^{-n} for n greater than one are indicative of a Mott variable range hopping mechanism, where n = 2 corresponds to one-dimensional variable range hopping, n = 3 to two-dimensional variable range hopping, and n = 4 to three-dimensional variable range hopping, which is common in oxides.[60] The inset shown in Figure 8 is near linear, indicating thermally activated conduction in the titled material. To rule out Mott variable range hopping as a possible transport mechanism, Ln ρ was plotted against T^{-4} and a significant deviation from linearity was observed, shown in Figure S1.
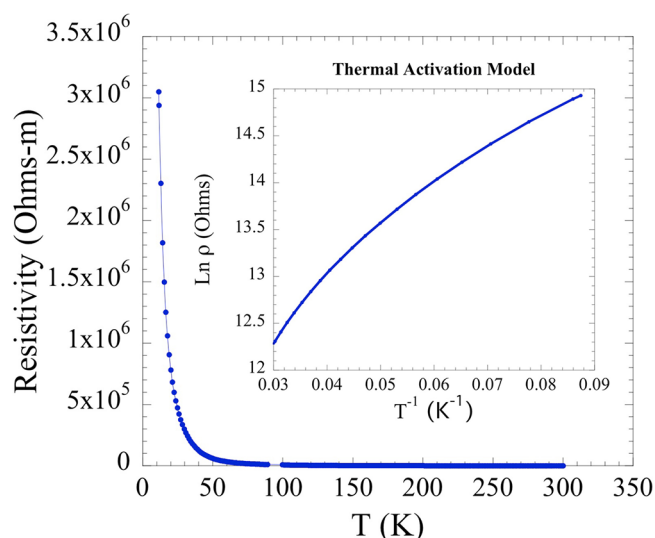
Figure 8. Temperature dependence of the electrical resistivity for the composition Ba$_3$Fe$_{1.56}$Ir$_{1.44}$O$_9$. The inset depicts the natural logarithm of electrical resistance plotted against inverse temperature, indicating thermally activated conduction. The gap in the resistivity data around 100 K is the result of temporary loss of electrical contact, and the data were excluded.

To determine the suitability of the titled material for ferroelectric measurements, the voltage dependence of an applied current was measured on single crystals, with the results shown in Figure 9. Given the 1.2 mm size of the single crystal
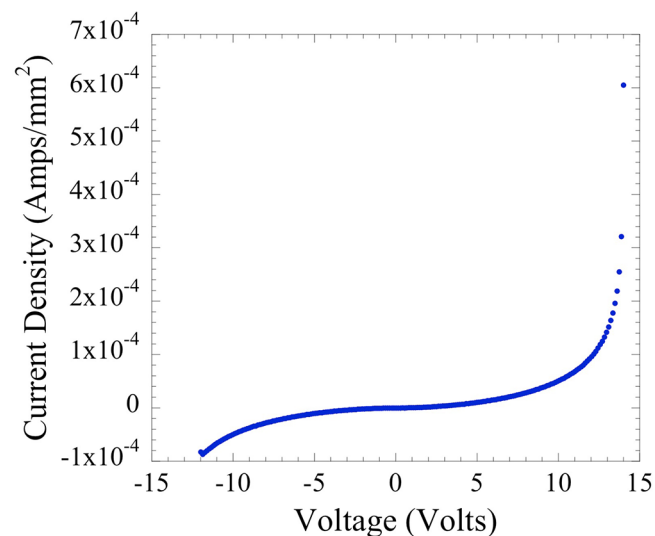
Figure 9. Electrical current density plotted against voltage for single crystals of Ba$_3$Fe$_{1.56}$Ir$_{1.44}$O$_9$.

measured, and the relatively low observed current as a function of voltage, a linear dependence up to at least 200 V is necessary to achieve sufficiently large currents to test for ferroelectric switching. The measured IV curve indicates highly nonlinear behavior, with an exponential increase in current at only 14 V. As a result, any ferroelectric measurement would only be able to sweep roughly 10 V, which corresponds to an extremely small electric field (0.1 kV/cm) for a crystal of this size, and for these reasons ferroelectric measurements were not conducted. However, since switching fields of ferroelectric oxides are

typically at least in the order of several kV/cm, we cannot exclude the presence of ferroelectric polarization in the crystals.

Density Functional Theory. The electronic structure of the $Fe1O_6$ polyhedra possessing local C_{3v} symmetry in the titled material, the only site in this structure that was fully occupied, was investigated by the DFT calculations, shown in Figure 10. This result was compared against the calculated
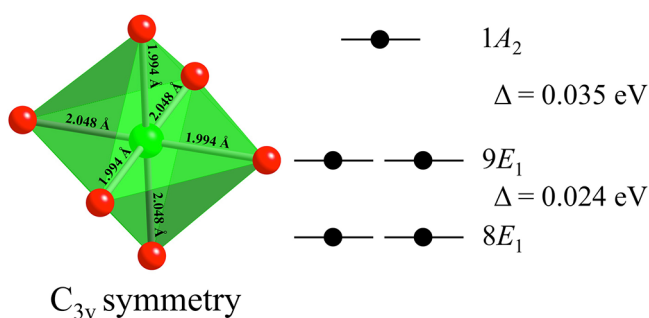
Figure 10. Density functional theory calculation of the crystal field splitting of a FeO_6 polyhedron with local C_{3v} symmetry.

0.032 eV for the split between t_{2g} and e_g for a FeO_6 possessing O_h symmetry, suggesting the energetic possibility of Fe(III) in this structure to manifest as an $S = 5/2$ cation. The energetic gaps between orbitals $8E_1$ and $9E_1$, and $9E_1$ and $1A_2$, respectively, are close to the calculated energy gap between the more commonly observed t_{2g} and e_g in O_h symmetry polyhedra, supporting this possibility. Two structurally similar iron containing oxides of the $LiNbO_3$-type with identical local C_{3v} symmetry FeO_6 polyhedra, $MFeO_3$ (M = Ga, Sc) were investigated by neutron diffraction and Mössbauer spectroscopy, confirming the presence of a $S = 5/2$ electronic configuration in both cases, corroborating our calculations.[61,62]

Mössbauer Measurements. Room temperature zero-field Mössbauer spectroscopy of $Ba_3Fe_{1.56}Ir_{1.44}O_9$ was measured, shown in Figure 11. The spectrum consists of a single, well-
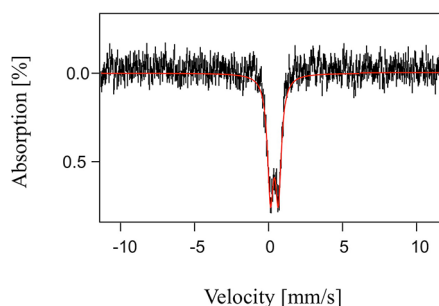
Figure 11. Room temperature zero-field Mössbauer spectrum of $Ba_3Fe_{1.56}Ir_{1.44}O_9$.

defined quadrupole doublet. This data is characterized by an isomer shift $\delta = 0.39(1)$ mm/s, quadrupole splitting $\Delta E_Q = 0.54(1)$ mm/s, and relative broad line widths, $\Gamma = 0.48(1)$ mm/s. These parameters are typical of high spin Fe(III) sites, consistent with compositions containing similar Fe(III) environments, such as $GaFeO_3$ and $ScFeO_3$. The observation of Fe(III) further corroborates our BVS and XANES assignments of Fe(III) in this composition.

Magnetic Properties. The temperature dependence of the magnetic susceptibility under an applied field of 0.1 T is shown in Figure 12, along with a pure powder X-ray diffraction pattern
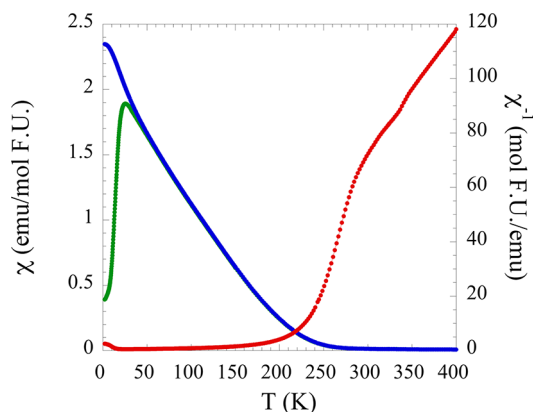
Figure 12. Temperature dependence of the magnetic susceptibility for $Ba_3Fe_{1.56}Ir_{1.44}O_9$ under an applied field of 0.1 T, with FC data shown in blue, ZFC data shown in green, and inverse susceptibility data shown in red.

shown in Figure S2. Significant field dependence is observed at 55 K, with a full order of magnitude difference in susceptibility between the FC and ZFC measurements. There is a sharp antiferromagnetic transition at 50 K in the ZFC followed by a significantly higher ferromagnetic-like transition at $T_N = 270$ K, in addition to a broader transition at $T_N = 340$ K. A fit of the high temperature inverse susceptibility data (with an added temperature independent parameter $\chi_0 = 0.005$), shown in Figure S3, suggests an effective moment of 4.07 μ_B, which differs significantly from the spin only moment of 7.39 μ_B, calculated by treating Fe(III) as a $S = 5/2$ magnetic cation and Ir(V) as nonmagnetic, consistent with previous reports of Ir(V) containing oxides.[48] The large difference between effective and calculated moments can be explained by the presence of multiple high temperature magnetic transitions. The fit of the high temperature inverse susceptibility data that was used to determine an effective moment is too close in temperature to the nearest magnetic transition, suggesting that this range is not in the Curie−Weiss regime and thus does not yield an accurate effective moment. The temperature dependence of $\chi_m T$ under an applied field of 0.1 T, shown in Figure S4, corroborates the ferromagnetic-like behavior of $Ba_3Fe_{1.56}Ir_{1.44}O_9$ observed in the temperature sweep measurements and indicates a magnetic moment of 5.20 μ_B. The broad transition at $T_N = 270$ K in the temperature sweep data is clearly shown as the onset of ferromagnetic-like order in this $\chi_m T$ plot. A measurement at higher temperature is needed to obtain an accurate effective moment in the Curie−Weiss regime.

The temperature dependence of the magnetic susceptibility under an applied field of 1 T, shown in Figure S5, exhibits an order of magnitude decrease in magnetic susceptibility compared to the 0.1 T data. Although the field dependence was decreased, the temperature of the divergence onset was increased to 180 K, and a low temperature antiferromagnetic-like transition is exhibited in the FC data. This transition was observed in the ZFC for the 0.1 T data, suggesting a complex field dependence relationship in this material. Magnetization versus field measurements were taken at both 2 and 45 K, shown in Figure S6−7, exhibiting weak hysteresis.

■ CONCLUSION

A noncentrosymmetric polar, site-disordered trigonal triple perovskite, $Ba_3Fe_{1.56}Ir_{1.44}O_9$, was grown as single crystals from a

molten carbonate flux. The oxidation states were determined to be Fe(III) and Ir(V) by BVS analysis and XANES measurement, using $Ba_3NiIr_2O_9$ as a XANES reference material for Ir(V) in a triple perovskite structure. Electrical conductivity data consistent with semiconducting behavior were observed, and the transport mechanism was best described as thermally activated. Voltage dependent current curves exhibited significant deviation from linearity, indicating that the material was unsuitable for ferroelectric measurements, despite the polar structure. The effect of the trigonal distortion on the crystal field splitting of $Fe(III)O_6$ was investigated via density functional theory calculations, and the spin state of iron was determined to be S = 5/2. Magnetic properties were measured and a near room temperature (T_N = 270 K) ferromagnetic-like transition was observed.

■ ASSOCIATED CONTENT

Ⓢ Supporting Information

The Supporting Information is available free of charge on the ACS Publications website at DOI: 10.1021/acs.inorgchem.8b01015.

> Temperature dependent electrical resistance, temperature dependent magnetic susceptibility, field dependent magnetization (PDF)

Accession Codes

CCDC 1823084−1823085 contain the supplementary crystallographic data for this paper. These data can be obtained free of charge via www.ccdc.cam.ac.uk/data_request/cif, or by emailing data_request@ccdc.cam.ac.uk, or by contacting The Cambridge Crystallographic Data Centre, 12 Union Road, Cambridge CB2 1EZ, UK; fax: +44 1223 336033.

■ AUTHOR INFORMATION

Corresponding Author

*E-mail: zurloye@mailbox.sc.edu. Phone: (803) 777-6916. Fax: (803) 777-8508.

ORCID Ⓘ

Steve M. Heald: 0000-0002-4369-8248
Gregory Morrison: 0000-0001-9674-9224
Hans-Conrad zur Loye: 0000-0001-7351-9098

Notes

The authors declare no competing financial interest.

■ ACKNOWLEDGMENTS

■ REFERENCES

(1) Rijssenbeek, J. T.; Huang, Q.; Erwin, R. W.; Zandbergen, H. W.; Cava, R. J. The Crystal Structure of $Ba_3CuRu_2O_9$ and Comparison to $Ba_3MRu_2O_9$ (M = In, Co, Ni, Fe). *J. Solid State Chem.* **1999**, *146*, 65−72.

(2) Doi, Y.; Hinatsu, Y. Magnetic and calorimetric studies on $Ba_3LnRu_2O_9$ (Ln = Gd, Ho-Yb) with 6H-perovskite structure. *J. Mater. Chem.* **2002**, *12*, 1792−1795.

(3) Kim, S.-J.; Smith, M. D.; Darriet, J.; zur Loye, H.-C. Crystal growth of new perovskite and perovskite related iridates: $Ba_3LiIr_2O_9$, $Ba_3NaIr_2O_9$, and $Ba_{3.44}K_{1.56}Ir_2O_{12}$. *J. Solid State Chem.* **2004**, *177*, 1493−1500.

(4) Doi, Y.; Hinatsu, Y. The structural and magnetic characterization of 6H-perovskite-type oxides $Ba_3LnIr_2O_9$ (Ln = Y, lanthanides). *J. Phys.: Condens. Matter* **2004**, *16*, 2849−2860.

(5) Lufaso, M. W.; zur Loye, H.-C. Crystal Structures and Magnetic Properties of Mixed Iridium-Ruthenium Triple Perovskites. 1. $Ba_3MRuIrO_9$ (M = Lanthanide, Y). *Inorg. Chem.* **2005**, *44*, 9143−9153.

(6) Lufaso, M. W.; zur Loye, H.-C. Crystal Structures and Magnetic Properties of Mixed Iridium-Ruthenium Triple Perovskites. 2. $Ba_3MRuIrO_9$ (M = Li, Na, Mg, Ni, Zn, Bi, In). *Inorg. Chem.* **2005**, *44*, 9154−9161.

(7) Sakamoto, T.; Doi, Y.; Hinatsu, Y. Crystal structures and magnetic properties of 6H-perovskite-type oxides $Ba_3MIr_2O_9$ (M = Mg, Ca, Sc, Ti, Zn, Sr, Zr, Cd, In). *J. Solid State Chem.* **2006**, *179*, 2595−2601.

(8) zur Loye, H.-C.; Kim, S.-J.; Macquart, R.; Smith, M. D.; Lee, Y.; Vogt, T. Low temperature structural phase transition of $Ba_3NaIr_2O_9$. *Solid State Sci.* **2009**, *11*, 608−613.

(9) Zhao, J. G.; Yang, L. X.; Yu, Y.; Li, F. Y.; Yu, R. C.; Jin, C. Q. Structural and physical properties of 1:2 B-site-ordered perovskite $Ba_3CaIr_2O_9$. *J. Solid State Chem.* **2009**, *182*, 327−330.

(10) Felder, J. B.; Yeon, J.; Smith, M. D.; zur Loye, H.-C. Compositional and Structural Versatility in an Unusual Family of anti-Perovskite Fluorides: $[Cu(H_2O)_4]_3[(MF_6)(M'F_6)]$. *Inorg. Chem.* **2016**, *55*, 7167−7175.

(11) Walker, H. C.; Mustonen, O.; Vasala, S.; Voneshen, D. J.; Le, M. D.; Adroja, D. T.; Karppinen, M. Spin wave excitations in the tetragonal double perovskite Sr_2CuWO_6. *Phys. Rev. B: Condens. Matter Mater. Phys.* **2016**, *94*, 064411.

(12) Luo, H. M.; Jain, M.; Baily, S. A.; McCleskey, T. M.; Burrell, A. K.; Bauer, E.; DePaula, R. F.; Dowden, P. C.; Civale, L.; Jia, Q. X. Structural and Ferromagnetic Properties of Epitaxial $SrRuO_3$ Thin Films Obtained by Polymer-Assisted Deposition. *J. Phys. Chem. B* **2007**, *111*, 7497−7500.

(13) Cohen, R. E. Origin of ferroelectricity in perovskite oxides. *Nature* **1992**, *358*, 136−138.

(14) Schneemeyer, L. F.; Waszczak, J. V.; Zahorak, S. M.; van Dover, R. B.; Siegrist, T. Superconductivity in rare earth cuprate perovskites. *Mater. Res. Bull.* **1987**, *22*, 1467−1473.

(15) Perez, J.; Stankiewicz, J.; Blasco, J.; Castro, M.; Garcia, J. The metal-insulator transition in $NdNi_{1-x}Cu_xO_3$. *J. Phys.: Condens. Matter* **1996**, *8*, 10393.

(16) Miiller, W.; Avdeev, M.; Zhou, Q.; Kennedy, B. J.; Sharma, N.; Kutteh, R.; Kearley, G. J.; Schmid, S.; Knight, K. S.; Blanchard, P. E. R.; Ling, C. D. Giant Magnetoelastic Effect at the Opening of a Spin-Gap in $Ba_3BiIr_2O_9$. *J. Am. Chem. Soc.* **2012**, *134*, 3265−3270.

(17) Geprags, S.; Opel, M.; Sebastian, T.; Goennenwein, B.; Gross, R. Giant magnetoelastic effects in $BaTiO_3$-based extrinsic multiferroic hybrids. *Phys. Rev. B: Condens. Matter Mater. Phys.* **2012**, *86*, 134432.

(18) Kemmler-Sack, V. S.; Ehmann, A. On $Ba_3FeIr_2O_{9-x}$. *Z. Anorg. Allg. Chem.* **1982**, *494*, 87−90.

(19) Treiber, V. U.; Kemmler-Sack, S.; Ehmann, A. Perovskites with Noble Metals of Type $Ba_3BM_2O_9$; B = Mg, Fe, Co, Ni, Zn, Cd; M = Ru, Ir. *Z. anorg. allg. Chem.* **1982**, *487*, 198.

(20) Rohweder, U.; Muller-Buschbaum, H. The Crystal Chemistry of $Mn_3ZnBb_2O_9$ and $MnZn_3Nb_2O_8$. *J. Less-Common Met.* **1988**, *142*, 75−83.

(21) Lightfoot, P.; Battle, P. D. The crystal and magnetic structures of $Ba_3NiRu_2O_9$, $Ba_3CoRu_2O_9$, and $Ba_3ZnRu_2O_9$. *J. Solid State Chem.* **1990**, *89*, 174−183.

(22) Stitzer, K. E.; Smith, M. D.; Gemmill, W. R.; zur Loye, H.-C. Novel Mixed-Valent (V/VI) Triple Perovskite Ruthenates: Observation of a Complex Low-Temperature Structural and Magnetic Transition. *J. Am. Chem. Soc.* **2002**, *124*, 13877−13885.

(23) Stitzer, K. E.; El Abed, A.; Smith, M. D.; Davis, M. J.; Kim, S.-J.; Darriet, J.; zur Loye, H.-C. Crystal Growth of Novel Osmium-Containing Triple Perovskites. *Inorg. Chem.* **2003**, *42*, 947−949.

(24) Jordan, N. A.; Battle, P. D.; Sloan, J.; Manuel, P.; Kilcoyne, S. Structural chemistry and magnetic properties of 6H and 15R hexagonal perovskites $BaIr_xFe_{1-x}O_3$-delta. *J. Mater. Chem.* **2003**, *13*, 2617−2625.

(25) Mogare, K. M.; Klein, W.; Jansen, M. $K_2NaOsO_{5.5}$ and $K_3NaOs_2O_9$: The first osmium perovskite containing alkali metal cations at the "A" site. *J. Solid State Chem.* **2012**, *191*, 153−157.

(26) Albornoz, J. C.; Landinez Tellez, D. A.; Roa-Rojas, J.; Munevar, J. A.; Baggio-Saitovich, E. Structural and Magnetic Properties of the New $La_2SrCo_2FeO_9$ Triple Perovskite. *J. Supercond. Novel Magn.* **2013**, *26*, 2313−2317.

(27) Huang, Z.; Aukett, J. E.; Blanchard, P. E. R.; Kennedy, B. J.; Miiler, W.; Zhou, Q.; Avdeev, M.; Johnson, M. R.; Zbiri, M.; Garbarino, G.; Marshall, W. G.; Gu, Q.; Ling, C. D. Pressure-Induced Intersite Bi-M (M = Ru, Ir) Valence Transitions in Hexagonal Perovskites. *Angew. Chem.* **2014**, *126*, 3482−3485.

(28) Beran, P.; Ivanov, S. A.; Nordblad, P.; Middey, S.; Sarman, D. D.; Ray, S.; Mathieu, R. Neutron powder diffraction study of $Ba_3ZnRu_{2-x}Ir_xO_9$ (x = 0,1,2) with 6H-type perovskite structure. *Solid State Sci.* **2015**, *50*, 58−64.

(29) Casallas, F.; Vera, E.; Landinez, D.; Parra, C.; Roa, J. Structural properties, electric response and magnetic behaviour of $La_2SrFe_2CoO_9$ triple complex perovskite. *J. Phys.: Conf. Ser.* **2016**, *687*, 012047.

(30) Quilliam, J. A.; Bert, F.; Manseau, A.; Darie, C.; Guillot-Deudon, C.; Payen, C.; Baines, C.; Amato, A.; Mendels, P. Gapless quantum spin liquid ground state in the spin-1 antiferromagnetic 6HB-$Ba_3NiSb_2O_9$. *Phys. Rev. B: Condens. Matter Mater. Phys.* **2016**, *93*, 214432.

(31) Jiao, L.; Xu, J.; Li, Z.; Wang, J.-F.; Zhou, J.; Gu, Z.-B.; Zhang, S.-T. Room temperature ferromagnetism in triple perovskite $Sr_3CrFeMO_9$. *J. Mater. Sci.: Mater. Electron.* **2013**, *24*, 4970−4973.

(32) Stitzer, K. E.; El Abed, A.; Darriet, J.; zur Loye, H.-C. Crystal Growth and Structure Determination of Barium Rhodates: Stepping Stones toward 2H-$BaRhO_3$. *J. Am. Chem. Soc.* **2004**, *126*, 856−864.

(33) Davis, M. J.; Mugavero, S. J.; Glab, K. I.; Smith, M. D.; zur Loye, H.-C. The crystal growth and characterization of the lanthanide-containing double perovskites Ln_2NaIrO_6 (Ln = La, Pr, Nd). *Solid State Sci.* **2004**, *6*, 413−417.

(34) Macquart, R.; Kim, S.-J.; Gemmill, W. R.; Stalick, J. K.; Lee, Y.; Vogt, T.; zur Loye, H.-C. Synthesis, Structure, and Magnetic Properties of Sr_2NiOsO_6 and Ca_2NiOsO_6: Two New Osmium-Containing Double Perovskites. *Inorg. Chem.* **2005**, *44*, 9676−9683.

(35) Mugavero, S. J.; Smith, M. D.; zur Loye, H.-C. The crystal growth and magnetic properties of Ln_2LiIrO_6 (Ln = La, Pr, Nd, Sm, Eu). *J. Solid State Chem.* **2005**, *178*, 200−206.

(36) Gemmill, W. R.; Smith, M. D.; zur Loye, H.-C. Synthesis and structural characterization of two new hexagonal osmates: $Ba_3Fe_{0.92}Os_{1.08}O_6$ and $Ba_2Co_{0.77}Os_{1.23}O_6$. *Solid State Sci.* **2007**, *9*, 380−384.

(37) Mugavero, S. J.; Gemmill, W. R.; Roof, I. P.; zur Loye, H.-C. Materials discovery by crystal growth: Lanthanide metal containing oxides of the platinum group metals (Ru, Os, Ir, Rh, Pd, Pt) from molten alkali metal hydroxides. *J. Solid State Chem.* **2009**, *182*, 1950−1963.

(38) Ferreira, T.; Morrison, G.; Jeongho, Y.; zur Loye, H.-C. Crystal growth of incommensurate members of 2H-hexagonal perovskite related oxides: $Ba_4M_zPt_{3-z}O_9$ (M = Co, Ni, Cu, Zn, Mg, Pt). *J. Solid State Chem.* **2016**, *236*, 2−9.

(39) Ferreira, T.; Morrison, G.; Jeongho, Y.; zur Loye, H.-C. Design and Crystal Growth of Magnetic Double Perovskite Iridates: Ln_2MIrO_6 (Ln = La, Pr, Nd, Sm-Gd; M = Mg, Ni). *Cryst. Growth Des.* **2016**, *16*, 2795−2803.

(40) Middey, S.; Aich, P.; Meneghini, C.; Mukherjee, K.; Sampathkumaran, E. V.; Siruguri, V.; Mahadevan, P.; Ray, S. Metal-insulator transition in $Ba_3Fe_{1-x}Ru_{2+x}O_9$: Interplay between site disorder, chemical percolation, and electronic structure. *Phys. Rev. B: Condens. Matter Mater. Phys.* **2016**, *94*, 184424.

(41) Dey, T.; Majumder, M.; Orain, J. C.; Senyshyn, A.; Prinz-Zwick, M.; Bachus, S.; Tokiwa, Y.; Bert, F.; Khuntia, P.; Buttgen, N.; Tsirlin, A. A.; Gegenwart, P. Persistent low-temperature spin dyanmics in the mixed-valence iridate $Ba_3InIr_2O_9$. *Phys. Rev. B: Condens. Matter Mater. Phys.* **2017**, *96*, 174411.

(42) Ferreira, T.; Heald, S. M.; Smith, M. D.; zur Loye, H.-C. Unusual Coexistence of Nickel(II) and Nickel(IV) in the Quadruple Perovskite $Ba_4Ni_2Ir_2O_{12}$ Containing Ir_2NiO_{12} Mixed-Metal-Cation Trimers. *Inorg. Chem.* **2018**, *57*, 2973−2976.

(43) Buller-Buschbaum, H. On the Crystal Chemistry of Oxoiridates. *Z. Anorg. Allg. Chem.* **2005**, *631*, 1005−1028.

(44) Okamoto, Y.; Nohara, M.; Aruga-Katori, H.; Takagi, H. Spin-Liquid State in the S = 1/2 Hyperkagome Antiferromagnet $Na_4Ir_3O_8$. *Phys. Rev. Lett.* **2007**, *99*, 137207.

(45) Kim, B. J.; Jin, H.; Moon, S. J.; Kim, J.-Y.; Park, B.-G.; Leem, C. S.; Yu, J.; Noh, T. W.; Kim, C.; Oh, S.-J.; Park, J.-H.; Durairaj, V.; Cao, G.; Rotenberg, E. Novel Jeff = 1/2 Mott State Induced by Relativistic Spin-Orbit Coupling in Sr_2IrO_4. *Phys. Rev. Lett.* **2008**, *101*, 076402.

(46) Kim, B. J.; Ohsumi, H.; Komesu, T.; Sakai, S.; Morita, T.; Takagi, H.; Arima, T. Phase-Sensitive Observation of a Spin-Orbital Mott State in Sr_2IrO_4. *Science* **2009**, *323*, 1329−1332.

(47) Pesin, D.; Balents, L. Mott physics and band topology in materials with strong spin-orbit interaction. *Nat. Phys.* **2010**, *6*, 376−381.

(48) Laguna-Marco, M. A.; Kayser, P.; Alonso, J. A.; Martinez-Lope, M. J.; van Veenendaal, M.; Choi, Y.; Haskel, D. Electronic structure, local magnetism, and spin-orbit effects of Ir(IV)-,Ir(V)-, and Ir(VI)-based compounds. *Phys. Rev. B: Condens. Matter Mater. Phys.* **2015**, *91*, 214433.

(49) Sheldrick, G. M. A short history of SHELX. *Acta Crystallogr., Sect. A: Found. Crystallogr.* **2008**, *A64*, 112−122.

(50) Hubschle, C. B.; Sheldrick, G. M.; Dittrich, B. ShelXle: a Qt graphical user interface for SHELXL. *J. Appl. Crystallogr.* **2011**, *44*, 1281−1284.

(51) Le Page, Y. Computer derivation of the symmetry elements implied in a structure description. *J. Appl. Crystallogr.* **1987**, *20*, 264−269.

(52) te Velde, G.; Bickelhaupt, F. M.; Baerends, E. J.; Fonseca Guerra, C.; van Gisbergen, S. J. A.; Snijders, J. G.; Ziegler, T. Chemistry with ADF. *J. Comput. Chem.* **2001**, *22*, 931−967.

(53) Perdew, J. P.; Ruzsinszky, A.; Csonka, G. I.; Vydrov, O. A.; Scuseria, G. E.; Constantin, L. A.; Zhou, X.; Burke, K. Restoring the Density-Gradient Expansion for Exchange in Solids and Surfaces. *Phys. Rev. Lett.* **2008**, *100*, 136406.

(54) Morrison, G.; zur Loye, H.-C. Simple correction for the sample shape and radial offset effects on SQUID magnetometers: Magnetic measurements on Ln_2O_3 (Ln = Gd, Dy, Er) standards. *J. Solid State Chem.* **2015**, *21*, 333−337.

(55) Glazer, A. M.; Stadnicka, K. On the use of the term 'absolute' in crystallography. *Acta Crystallogr., Sect. A: Found. Crystallogr.* **1989**, *A45*, 234−238.

(56) Halasyamani, P. S.; Poeppelmeier, R. Noncentrosymmetric Oxides. *Chem. Mater.* **1998**, *10*, 2753−2769.

(57) Eerenstein, W.; Mathur, N. D.; Scott, J. F. Multiferroic and magnetoelectric materials. *Nature* **2006**, *442*, 759−765.

(58) Khomskii, D. I. Multiferroics: Different ways to combine magnetism and ferroelectricity. *J. Magn. Magn. Mater.* **2006**, *306*, 1−8.

(59) Mugavero, S. J., III; Smith, M. D.; Yoon, W.-S.; zur Loye, H.-C. $Nd_2K_2IrO_7$ and $Sm_2K_2IrO_7$: Iridium (VI) Oxides Prepared under Ambient Pressure. *Angew. Chem., Int. Ed.* **2009**, *48*, 215−218.

(60) Song, J.; Zhao, B.; Yin, L.; Qin, Y.; Zhou, J.; Wang, D.; Song, W.; Sun, Y. Reentrant spin glass behavior and magnetodielectric coupling of an Ir-based double perovskite compound, La_2CoIrO_6. *Dalton Trans.* **2017**, *46*, 11691−11697.

(61) Kawamoto, T.; Fujita, K.; Yamada, I.; Matoba, T.; Joo Kim, S.; Gao, P.; Pan, X.; Findlay, S. D.; Tassel, C.; Kageyama, H.; Studer, A. J.; Hester, J.; Irifune, T.; Akamatsu, H.; Tanaka, K. Room-Temperature Polar Ferromagnet $ScFeO_3$ Transformed from a High-Pressure Orthorhombic Perovskite Phase. *J. Am. Chem. Soc.* **2014**, *136*, 15291−15299.

(62) Niu, H.; Pitcher, M. J.; Corkett, A. J.; Ling, S.; Mandal, P.; Zanella, M.; Dawson, K.; Stamenov, P.; Batuk, D.; Abakumov, A. M.; Bull, C. J.; Smith, R. I.; Murray, C. A.; Day, S. J.; Slater, B.; Cora, F.; Claridge, J. B.; Rosseinsky, M. J. Room Temperature Magnetically Ordered Polar Corundum $GaFeO_3$ Displaying Magnetoelectric Coupling. *J. Am. Chem. Soc.* **2017**, *139*, 1520−1531.